

Direction-Dependent Properties in Inverted Carbon Nitride Colloidal Glasses with Gradient Porosity

*Jochen Bahner^[b], Lukas Dobler^[b], Marvin Frisch^[b,c], Lars Vogelsang^[b], Helmut Cölfen^[b] and Sebastian Polarz^[a,b]**

[a] Prof. Dr. S. Polarz
Leibniz-University Hannover, Institute of Inorganic Chemistry, Callinstrasse 9, 30167
Hannover, Germany
E-mail: sebastian.polarz@aca.uni-hannover.de

[b] J. Bahner, L. Dobler, M. Frisch, L. Vogelsang, Prof. Dr. H. Cölfen, Prof. Dr. S. Polarz
University Konstanz, Department of Chemistry, Universitätsstrasse 10, 78457 Konstanz,
Germany

[c] M. Frisch
Technical University of Berlin, Department of Technical Chemistry, Strasse des 17. Juni 124,
10623 Berlin, Germany

Keywords: Functional Gradient Materials; Porous Materials; Carbon Nitride; Inverted Opals; Analytical Ultracentrifugation

Abstract: It is well known that the step from a dense packing of colloidal beads to the inverted systems was important for the optimization of photonic crystal properties. Inverted opals made of high-refractive index semiconductors have attracted great attention due to their supreme optical features such as the occurrence of a photonic band-gap and because of an astonishing behavior in photocatalysis or for photovoltaics caused by so-called slow photons. It is much less known that photonic glasses, despite being disordered, exhibit unique optical properties too like random lasing or high-contrast structural colors. In analogy to opals and inverted opals, one can expect that inverted colloidal glasses may lead to an amplification of photonic properties as well or even to the emergence of unexpected features. An inverted photonic glass is characterized by a dense packing of monodisperse voids with colloidal dimensions without any long-range order. The preparation of inverse photonic glasses has rarely been reported by now and cases for materials composed of a semiconductor as a pore-wall material are unknown. The synthesis of porous carbon nitride (C_3N_4) with inverted colloidal glass structure is demonstrated here using a template approach. The formation of the template with glass-like order is achieved by analytical ultracentrifugation (AUZ) of size-selected silica colloids,

followed by infiltration of a precursor sol, transformation to carbon nitride and the final removal of the template. The use of AUZ is particularly important because it even allows to use a mixture of differently sized template particles, which are gradually fractionated. Monoliths with optimized morphological features exhibiting a gradient porosity and highly accessible pores are obtained. The result are materials with a graded structure. What makes such functional gradient material interesting is, a dependence of the optical features on the position can be expected. In addition, the method presented here allows to synthesize materials with adjustable composition ranging from carbon over nitrogen-doped carbon to C_3N_4 with either graphitic or polymeric structure. Therefore, the optical band gap is highly adjustable and tunable with regards to the photonic properties, as confirmed by optical absorption and photoluminescence measurements.

1. Introduction

Emerging energy technologies ask for a precise control over the functionality and morphology of porous solids.^[1] Within this class of compounds, the tailored combination of various pore sizes with different network-building materials has led to improved functional properties for a plethora of applications like catalysis and separation.^[2] The optimization of porosity for sustainability and better performance in the field of energy conversion and storage are among the most promising fields of research in material chemistry.^[1b, 3] The synthesis of porous materials is mainly realized using so-called nanocasting processes employing colloidal or self-assembled templates.^[4] As most templating nanoparticles form colloidal crystals during assembly, dielectric structures, called photonic crystals, with a photonic band structure are formed.^[5] This property is maintained respectively even improved if the structures are inverted into a porous material, as it is a result of the periodically changing refractive index of the materials dictated by their structure.^[6] The synthesis of these so called inverse opals can be realized by infiltrating preformed colloidal templates with network forming precursors resulting

in promising applications, for example as sensors, in photovoltaics or in batteries.^[7] Especially the synthesis of semiconductors, mainly titanium dioxide (TiO₂), has drawn intensive interest in research, as the photonic band structure can enhance the photocatalytic activity.^[8] Besides the advantageous high accessible surface of porous materials in general, the periodically changing refractive index between the network forming TiO₂ and air filled voids leads to enhanced properties in photocatalysis.^[9] This leads to a localization of the light in the high refractive index TiO₂^[10], enhanced light harvesting by light trapping^[11] as well as the slow photon effect^[12]. An impressive study was reported by Low *et al.* using layered TiO₂ inverse opals with varying pore sizes for the photocatalytic CO₂ reduction. The combination of two different photonic structures resulted in a significantly enhanced catalytic activity due to improved light harvesting.^[13]

In contrast to highly ordered photonic crystals, the experimental realization of amorphous structured photonic glasses has been rarely reported.^[14] While special photonic properties like random lasing^[15], isotropic structural color^[16] and Anderson localization of light^[17] have been described for colloidal photonic glasses^[18], few investigations on the inverted porous structures have been performed. While some process has been made towards inverted photonic glasses consisting of ceramics^[19] or polymers^[20], the investigation of the properties is focused towards structural colour and therefore isolating materials.^[21] Because of the correlation between the photonic band structure as a function of the opal structure and the electronic gap and related properties of the semiconductor material, it could be highly interesting to obtain materials with pore features as a function of position.

However, the vast majority of research in porous materials in general and in inverted opals in particular focuses on a statistical distribution of all structural and functional features, resulting in homogeneity. If properties of a material are not separated by a sharp boundary, but gradually change into a spatial direction, so called functional gradient materials (FGMs) are formed.^[22] The field of FGMs is quite well researched for materials exhibiting functional chemical

gradients^[23] with promising applications for instance in the synthesis of tailored adhesive coatings^[24] or in separation science^[25]. Materials characterized by a gradually changing porosity are common in nature, e.g. in bones^[26], leading to their high mechanical stability, low density and highly accessible pores.^[27] The synthesis of such materials has been reported for large pores ($> 10 \mu\text{m}$) with applications e.g. in tissue engineering^[28] or electrophoresis^[29]. Applied methods include 3D printing^[30], emulsion templating^[31] or freeze-casting^[32]. Stubenrauch and co-workers reported another innovative pathway.^[33] Using a self-build combination of microfluidics and an extrusion printer, polymer hydrogels and their composites are synthesized with gradually changing pore sizes between 80 and 800 μm . For gradients including smaller pores in the nanometer regime, a selective swelling of copolymers can be employed.^[34] However, the experimental realization of well-defined gradients in macroscopic materials is challenging. The main limitation is the demanding generation of suitable templates, as well as their infiltration. A promising pathway to overcome this problem is the application of gradient centrifugation, which has seen a rise in research towards the structuration of colloidal assembly.^[35] While significant advances have been made on the understanding of the assembly behavior of monodisperse spheres under centrifugal force,^[36] the occurrence of non-dense structures with large scale gradients in particle sizes has scarcely been reported.^[35b] Our group has reported the possibility of creating various ordered as well as gradually changing structures when ultracentrifugation was used to assemble binary mixtures of polystyrene nanoparticles.^[37] This behavior could be adapted towards a templating process, resulting in the first synthesis of a gradient porous carbon material with pores on the nanoscale, which showed direction dependent enhanced functional properties when applied as electrode in lithium-oxygen batteries.^[38] Based on the latter publication and the arguments given for graded inverted opals, we ask if the method can be used for the generation of materials composed of a semiconductor as well.

Carbon nitride (C_3N_4) is a semiconductor, which is obviously strongly related to carbon materials. It is known, that carbon materials can be tuned by the incorporation of heteroatoms into the carbon network.^[39] The most discussed dopant is nitrogen due to the fact that the control over the degree of incorporation into the carbon network allows the adjustment of the functional properties for various applications, such as catalytic activity in electrochemistry or adsorption capacity for CO_2 -capture.^[40] Low to medium doping levels of nitrogen into carbon can lead to highly active electrocatalysts applicable towards the oxygen reduction reaction in lithium-based batteries^[41] or the electro-reduction of carbon dioxide^[42]. At very high levels of nitrogen incorporated into the carbon network, C_3N_4 is formed. The family of C_3N_4 derived compounds is characterized by a visible band gap which can be adjusted in the range of $\sim 1.4 - 2.8$ eV depending on the stoichiometric composition^[43] and crystalline structure^[44]. C_3N_4 attracts additional significant interest in research as it is eco-friendly, cheap and stable.^[45] Additionally, the energy levels of valence and conduction bands are suitable for hydrogen (H_2) generation and for Z-scheme based photocatalytic water purification. Therefore, applications in these fields are currently rising.^[46] Especially the control over the pore sizes and structures leads to enhanced photocatalytic properties, in example for water splitting or CO_2 reduction.^[46d, 47] Several researchers have already made notable progress on porous C_3N_4 materials. For instance, Liang *et al.* used monolithic porous C_3N_4 as catalyst for photocatalytic water splitting.^[48] The enhanced turnover rate of the macroscopic structure was attributed to a better light capture, charge separation and mass diffusion, which could be further improved in monoliths with an ordered porosity as reported by Sun and coworkers.^[49]

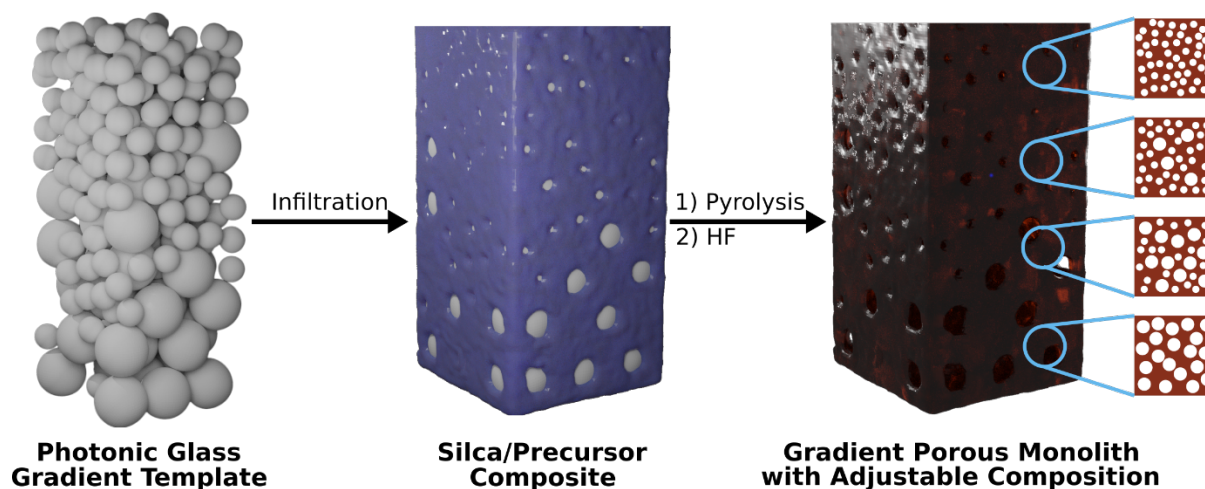
In a recent paper^[50], we showed that nitrogen and other dopants can be introduced into the pure carbon materials described before^[38]. The nitrogen atoms were introduced by the template particles, e.g. poly-aniline modified polystyrene lattices. However, our results showed clearly^[50], that the maximum amount of incorporated nitrogen is insufficient for the conversion to C_3N_4 . Therefore, we refrain from using template particles as nitrogen source, and present a

newly developed approach. Accordingly, inverted colloidal glasses consisting of the semiconductor C_3N_4 with a gradient structure in porosity can now be afforded. The paper is organized as follows. First, we will show how colloidal photonic glasses, consisting of differently sized silica nanoparticles (SiO_2 -NPs), can be formed using preparative ultracentrifugation (PUC). We will then present the applicability of these novel structures as templates for the generation of gradient porous materials. The infiltration of the structures with commercially available precursors will ultimately result in the first synthesis of gradient porous graphitic (g- C_3N_4) and polymeric (p- C_3N_4) carbon nitrides. Finally, the optical properties of the materials are studied.

2. Results and Discussion

As described before, we could successfully use binary mixtures of colloidal dispersions of two monodisperse polystyrene spheres (PS) for the co-assembly with a resorcinol-aldehyde (RA) precursor mixture using ultracentrifugation.^[38, 50-51] The desired carbon materials were obtained after crosslinking to a RA-gel followed by carbonization accompanied by thermal removal of PS. Our initial idea was to substitute the RA process by reactions, which are known from literature to end up in different carbon nitride compounds.^[44b, 52] Although, the conversion to carbon nitride materials was successful as shown for a guanidine-based approach in Supporting Information **Figure S1**, the structural information is lost entirely. Instead of an inverted opal structure, a porous agglomerate of ill-defined particles in the size-range 100 nm – 1 μ m was obtained according to scanning electron microscopy (SEM). Extensive work showed that PS latexes are unsuitable as templates. Therefore, we developed a more flexible approach as shown in **Scheme 1**. Using SiO_2 -nanoparticles (SiO_2 -NPs) results in the flexibility to tune the precursor composition (Supporting Information **Scheme S1**) towards the successful synthesis of

monolithic materials with compositions ranging from carbon over nitrogen doped carbon towards carbon nitride.



Scheme 1. Schematic illustration of the synthetic approach towards gradient porous monoliths with adjustable nitrogen contents. First, gradient templates are formed by ultracentrifugation. These can be infiltrated either *in situ* or by melt infiltration with different precursors as shown in **Scheme S1**. After a thermal conversion and template removal with hydrofluoric acid, gradient porous monoliths with adjustable compositions are yielded.

2.1. Ultracentrifugation-assisted construction of gradient templates composed of silica spheres.

Monodisperse spheres are also available for silica from the so-called Stöber method.^[53] The usage of colloidal glasses formed by SiO₂-NPs as templates offers several advantages. First, SiO₂-NPs can form stable dispersions in a wide range of precursor solutions. Second, SiO₂-NPs sediment in high density solutions, allowing for a precise control over the assembled structure. This was not possible using PS-NPs, which float on dense solvents when the solvent density exceeds 1.05 g/mL. Thus, we show results for the assembly behavior of binary mixtures of SiO₂-NPs inside centrifugal fields, resulting in the formation of gradient templates. We aim to create a slight separation between the particles, resulting in a gradual change in the local concentrations of the differently sized particles. Investigations of the assembly behavior of monodisperse colloids have drawn renewed interest in research^[35b] as colloidal assembly is a promising pathway towards the creation of nanoparticle-based materials.^[54] However, most

research is focused on the assembly into homogenous and highly ordered structures. The reason for this is, that contrary to intuition, the formation of highly ordered structures from monodisperse nanoparticles is much more favorable than our desired disordered gradient structure.^[14, 18, 37] We have prepared colloidal silica spheres with diameters of 129 ± 14 nm (denoted as SiO₂-129) and 310 ± 20 nm (denoted as SiO₂-310); the characterization is given in Supporting Information **Figure S2**. The assembly behavior under centrifugal force was then analyzed *in situ* using analytical ultracentrifugation (AUC), because recent studies have shown that AUC is very suitable to reveal information about the sedimentation of binary mixtures of small SiO₂-NPs.^[36b] It is worth noting that the pure SiO₂-129 and SiO₂-310 both show a typical sedimentation behavior expected for monodisperse samples. As shown in Supporting Information **Figure S3**, a constant decrease in nanoparticle concentration with increasing time of centrifugation can be observed. In contrast, the sedimentation behavior of binary mixtures of SiO₂-129 and SiO₂-310 presented in **Figure 1a** is characterized by the formation of a plateau in the local NP concentration separating the two steps representing each particle size. This is a clear indication of the temporal separation of the individual NPs sedimentation.

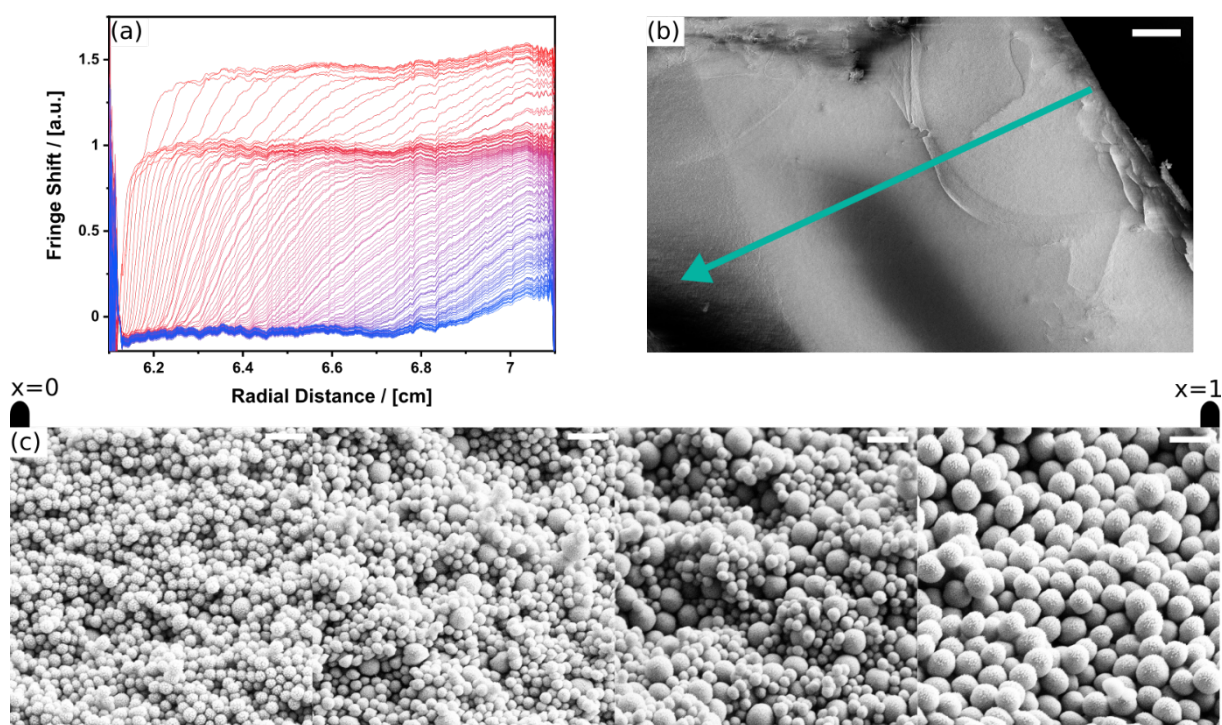


Figure 1. (a) Radial Rayleigh interference scans over time from red to blue in a sedimentation velocity run of a binary mixture of SiO₂-129 and SiO₂-310 at a rotational speed of 1500 rpm. The time interval between two scans is 120 s. SEM micrographs of (b) a Cross-section of silica opal with gradient in particle size, arrow indicating the direction of the gradient; scalebar = 50 μm and (c) micrographs taken along the gradient indicating the gradient in particle size; scalebar = 500 nm. Micrographs at lower magnifications given in the Supporting Information **Figure S4**.

In binary mixtures, SiO₂-310 completely and rapidly sediments within the first 30 min of centrifugation, as indicated by a decrease in maximal fringes above the plateau. A complete sedimentation of SiO₂-129 can only be observed after 150 min. However, a decrease in concentration of SiO₂-129, detectable by a slight loss in intensity at the plateau, is detected from the start of the sedimentation velocity experiment as an effect of radial dilution in the sector-shaped AUC centerpieces. In addition, sedimentation occurs only partially separated and a gradient formation seems possible. To further investigate this, we performed additional AUC measurements using UV-detection and compared them with simulations (see Supporting Information **Figure S3b**), confirming our findings of a gradual fractionation according to the particle size. Interactions between the different particle species can be excluded as the

hydrodynamic diameters calculated from the presented AUC data (see Supporting Information **Figure S3c**) are identical to the values determined from monomodal samples. As AUC is limited to highly diluted samples and therefore hardly applicable to the synthesis of macroscopic materials, we tested the transfer of the observed gradual separation to concentrated solutions and larger scales using PUC. After sedimentation of binary mixtures of SiO₂-129 and SiO₂-310 at intermediate centrifugal forces^[37], a monolithic colloidal structure with macroscopic dimensions as shown in **Figure 1b** was formed after drying. Using SEM, we investigated the structuration of the nanoparticles at distinct points along the direction of the centrifugal force indicated by the arrow in the cross-section. As predicted by AUC measurements, mixtures of SiO₂-129 and SiO₂-310 assemble in a gradient structure shown in **Figure 1c**. While the upper part of the monolith ($x \rightarrow 0$) is composed of only SiO₂-129, showing some degree of close-range order in an overall glassy state, the local fraction of SiO₂-310 increases gradually along the direction of the centrifugal force. Finally, in the lower part of the gradient structure ($x \rightarrow 1$) only large particles, again assembled in a glassy state, can be observed. For intermediate positions, no ordered aggregates are observed, indicating a kinetically driven assembly, overcoming the expected formation of ordered aggregates over the whole monolith (see also Supporting Information **Figure S4**).^[14, 55] The assembly behavior can easily be adjusted by the relative ratio of the individual particles and centrifugal force. At higher centrifugal forces, ordered structures of SiO₂-129 can be observed and no regions consisting of exclusively SiO₂-310 can be observed as the initial sedimentations occurs rapidly (see Supporting Information **Figure S5**).

2.2. Carbon nitride materials with gradient porosity.

The disordered, but dense packings of silica spheres presented in the last paragraph can now be used as templates (**Scheme 1**). The viability of the approach can be proven by using the silica

template instead of PS, but for the moment, for the preparation of a porous carbon material from a RA sol in analogy to ref. 38. During fractionation of the nanoparticles according to their size by PUC, the voids in the template are filled by the present precursor. After drying, the formed composite is converted to the final product by a single pyrolysis step. Gradient porous graphitic carbon materials were obtained successfully (see Supporting Information **Figure S6**). Beneficially, the detailed investigation of the infiltration and network forming process can be adopted towards the synthesis of a broader range of carbon-based materials with graded porosity, which was not possible using PS templates. Exemplarily, **Figure S7** shows the successful synthesis of highly graphitized carbon materials with gradient porosity using SiO₂-NPs dispersed in furfuryl alcohol. Lightly nitrogen doped carbons are accessible by infiltration with pyrrole acting as precursor and nitrogen doping agent simultaneously. However, the usage of disordered colloidal assemblies of SiO₂-NPs as templates offer possibilities in material design inaccessible until now. Due to the higher colloidal stability and density of SiO₂-NPs compared to PS, a temporal separation between the template formation step and the gelation of the precursor sol is feasible. Consequently, we can now use more demanding precursor sols, which is the key for the synthesis of materials with high nitrogen contents increasing from nitrogen-doped carbon (N@C) to C₃N₄ as shown in **Figure 2**. To achieve this, we dispersed binary mixtures of SiO₂-129 and SiO₂-310 in concentrated precursor solutions (see (I),(II) in Supporting Information **Scheme S1**), and fractionated the SiO₂-NPs by their size using PUC, followed by a thermal transformation step and removal of the SiO₂ template by HF etching. Depending on the nitrogen content of the precursor, either highly nitrogen doped carbon materials, further denoted as N@C (**Figure 2(a)**) or gradient porous g-C₃N₄ (**Figure 2(b)**) is yielded. A third possibility (III, Supporting Information **Scheme S1**) to synthesize gradient porous materials is melt infiltration. We covered the monolithic templates with 5-aminotetrazole (5AT). A slow heat up to 550 °C leads to an infiltration with molten 5AT

which then polymerizes to form p-C₃N₄ (**Figure 2(c)**). After etching with HF, orange monolithic p-C₃N₄ is obtained.

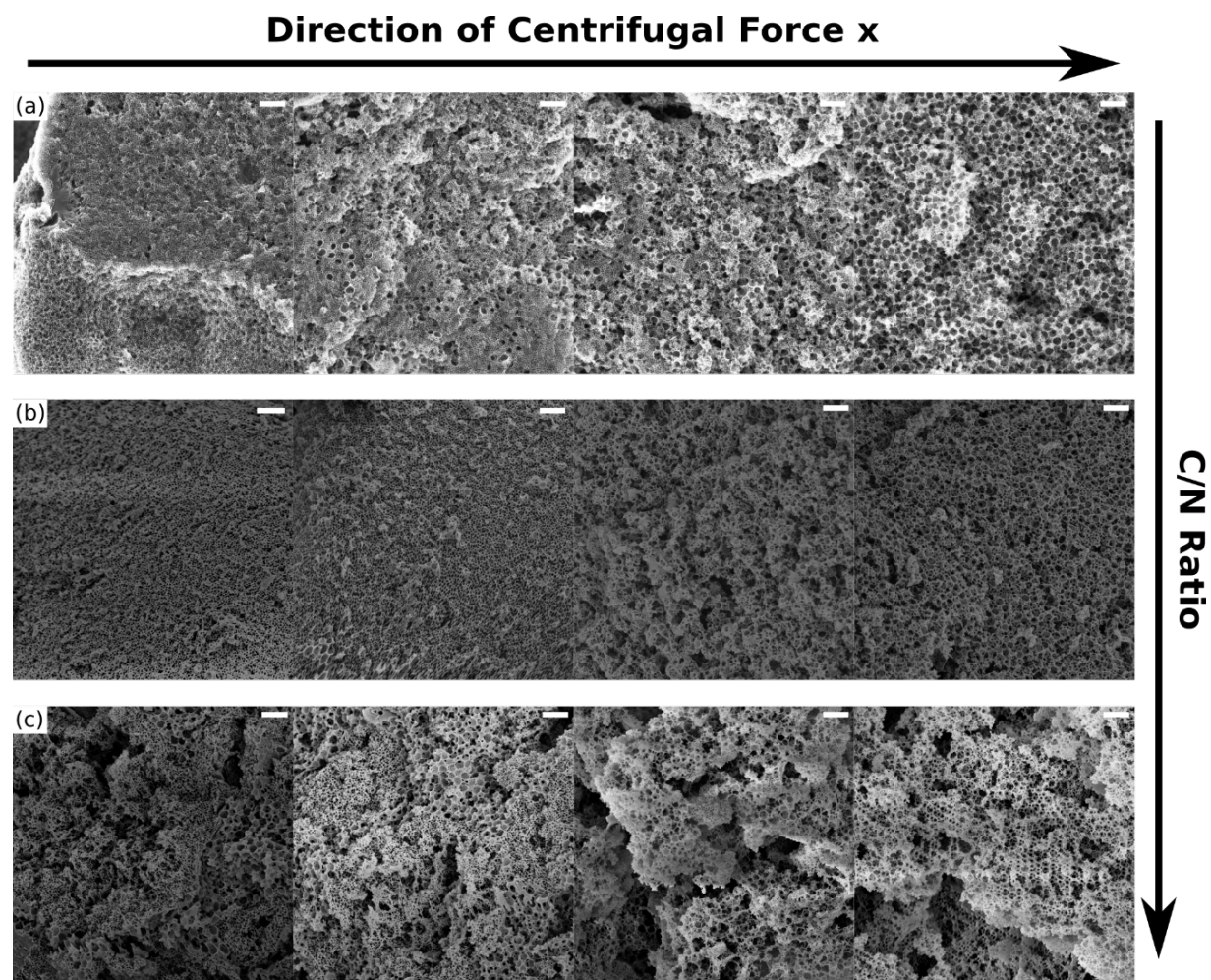


Figure 2. Gradient structure of inverted colloidal glasses with increasing nitrogen content from (a) to (c) as shown by subsequent SEM images taken along the internal coordinate x with scale bars of 1000 nm. SEM micrographs for (a) highly nitrogen doped carbons (C@N) (b) graphitic carbon nitride (g-C₃N₄) and (c) polymeric carbon nitride (p-C₃N₄).

All materials were yielded in a monolithic cylindrical shape with dimensions of ~ 0.7 cm and a gradient in pore sizes in the direction of the centrifugal force (~ 0.15 cm). The presence of the gradient structure can be proven by SEM micrographs as shown in **Figure 2**. Evidently, only smaller pores with a diameter of 88 ± 8 nm can be observed at the beginning of the gradient (left side, $x \rightarrow 0$). The portion of larger pores with average diameters of 316 ± 27 nm gradually increases towards the end of the gradient (right side, $x \rightarrow 1$). The accessibility of the internal

surface ($\sim 50 \text{ m}^2/\text{g}$) completely contributed by macroporous can be confirmed by N_2 -physisorption analysis (see Supporting Information **Figure S8**). This is further confirmed by recording higher magnified SEM micrographs given in **Figure S9** for all materials showing interconnected pores of uniform sizes. Importantly, the structural features do not significantly differ for the presented samples as evident by comparing the local pore sizes displayed for the individual samples presented in **Figure 2(a)-(c)** which is in accordance with the postulated formation process. To better compare the formed porosity gradients of the synthesized materials, we employed trainable Weka segmentation^[56] implemented in ImageJ^[57], as previously reported^[50-51]. This allows an objective calculation of the local area fraction of small pores, templated from SiO_2 -129 at specific positions x in the gradient region. As shown in **Figure 3**, all presented materials exhibit a gradual changing pore size along the gradient of the centrifugal force, confirming the analysis from SEM micrographs. Due to the different synthetic procedures, the density of the dispersion changes, resulting in a slight change in sedimentation coefficients and therefore gradient structure. This is evident as $\text{p-C}_3\text{N}_4$ (red curve in **Figure 3**), synthesized by melt infiltration shows a sharp transition between regions with predominantly small and large pores as observed during the investigation of the assembly process. In contrast, the gradient region is extended for C@N (black curve) and $\text{g-C}_3\text{N}_4$ (blue curve). This is a result of the high density of concentrated precursor solution, leading to a less pronounced fractionation, presenting an easy possibility to control the extension of the gradient region.

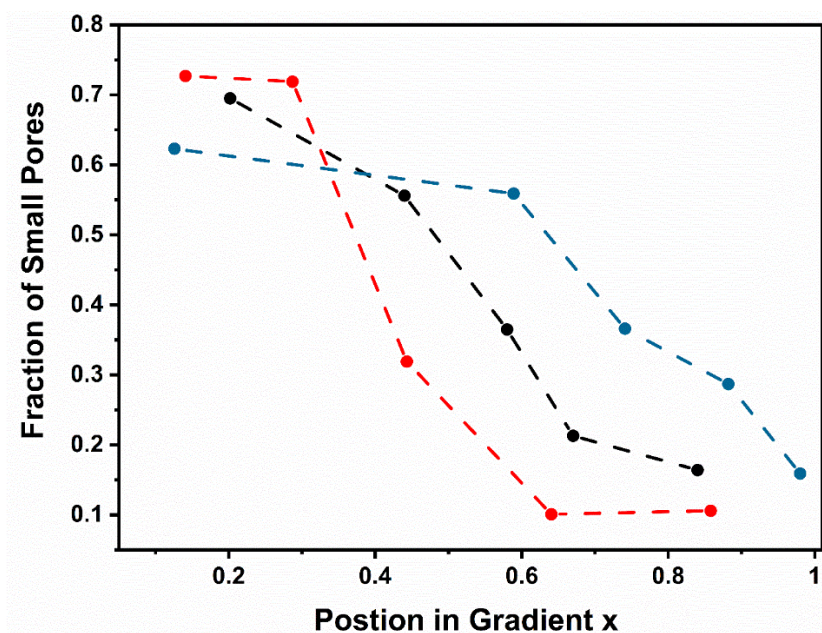


Figure 3: Correlation between the position in the gradient region and the calculated fraction of small pores according to WEKA image segmentation for C@N (black), g-C₃N₄ (blue) and p-C₃N₄ (red).

2.3. Chemical structure of the carbon nitride materials.

We know up to this point that monolithic glassy materials with the desired gradient porosity have been obtained by all presented methods, but it should be proven next, that the deliberately chosen methods lead to different kinds of materials. Therefore, a characterization of the chemical structure is necessary. First, we have investigated the network formation in the template's voids using thermogravimetric analysis (see Supporting Information **Figure S10**). For C@N (black curve), a stepwise mass loss is observed due to the elimination of water and ammonia during condensation reactions between 150 °C and 550 °C. The final formation of a graphitic carbon networks occurs during an isothermal treatment at 550 °C, resulting in the formation of a C@N-SiO₂-composite. A similar slow and stepwise condensation under cleavage of ammonia and water is observed during the formation process of g-C₃N₄ (blue curve) both synthesized after in situ infiltration. For p-C₃N₄ (red curve) synthesized by melt infiltration, a loss of water of crystallization from the precursor (5AT monohydrate) is detected at ~100 °C. Subsequently, the self-condensation of 5AT starts shortly after melting and infiltration at

~200 °C. After a rapid initial mass loss, the final p-C₃N₄/SiO₂ composite is formed after slower secondary condensation reactions and after an isothermal treatment at 550 °C. To clarify the underlying chemical processes leading to the network formation, we used ATR-IR given in **Figure 4**, and compared the spectra before and after pyrolysis. Besides the Si-O-Si-signal at 1051 cm⁻¹, strongly visible in all samples due to the presence of SiO₂-NPs, important insight into the process can be gained by an evaluation of the additional signals assignable to the precursor present in voids. In case of C@N (grey curve) strong signals are observed at 1668 cm⁻¹ corresponding to C=O vibrations and 1554 cm⁻¹ assignable to ring deformations in triazine units stemming from melamine. As only minor amine signals in the range of 3200 cm⁻¹ and 3600 cm⁻¹ are observable, we conclude that the precursor sol consisting of formaldehyde, guanidine, and melamine undergoes condensation reactions during drying of the composite resulting in a fixation of the precursor network.

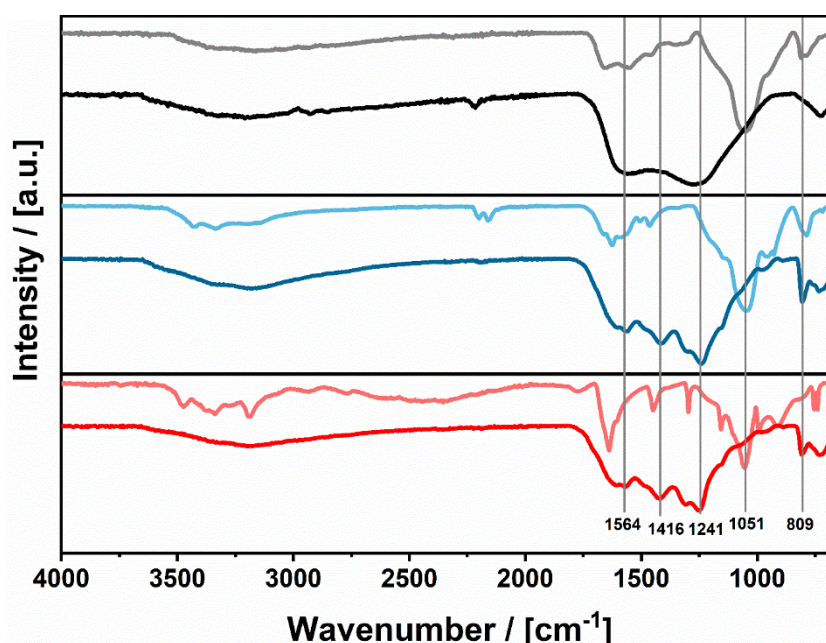


Figure 4: IR-spectra of the infiltrated precursor-SiO₂-composites (light curves) and the final gradient porous materials after template removal by HF etching (dark curves) for C@N (black), g-C₃N₄ (blue) and p-C₃N₄ (red).

Similar observations can be made for the synthesis of g-C₃N₄ synthesized using mixtures of urea and cyanamide. The dried infiltrated template (light blue curve) shows a reduced intensity for amine groups between 3334 cm⁻¹ and 3061 cm⁻¹ in the infiltrated template after drying in

comparison to untreated cyanamide (Supporting Information **Figure S11**). Additional C-N and C=N bonds are observable between 1633 cm^{-1} and 1459 cm^{-1} , indicating a self-condensation of cyanamide occurring during drying. The importance of these primary condensation reactions is shown by a comparison to the synthesis of C_3N_4 using only guanidine, which remains unchanged during drying (Supporting Information **Figure S12**), resulting in a collapse of the network due to an insufficient stability. Therefore, we derived two requirements for the synthesis of monolithic gradient porous materials using in situ infiltration during template formation. First, a primary reaction of the precursor must occur during drying of the composite yielded after fractionation to fix the structure. Second, the final matrix-building material must densely fill the template's voids. Otherwise, voids and cracks persist in the final structure leading to a collapse of the monolithic structure and therefore to a formation of porous powders. As expected, the situation is different for the p- C_3N_4 prepared by melt infiltration, showing a physical mixture of 5AT and silica before pyrolysis (light red curve). After pyrolysis and template removal by HF, the signal corresponding to Si-O-Si disappears in all presented samples (dark curves in **Figure 4**). This indicates a complete removal of the template, which is confirmed by Energy-dispersive X-ray spectroscopy (EDX, Supporting Information **Figure S13**) showing no remaining silicon signal.

The binding situation between carbon and nitrogen atoms as well as the ratio of carbon to nitrogen in the class of carbon/nitrogen-based solids is important to control the optical properties of the resulting materials.^[58] The synthetic method presented here allows the precise control of the resulting functionalities. The IR spectrum of N@C (black curve) is characterized by broad, overlaying signals between 1660 cm^{-1} and 1050 cm^{-1} assignable to various N-C and N=C bonds in heterocycles and C=C bonds stemming from the graphitic network. In contrast, g- C_3N_4 (blue curve) and porous p- C_3N_4 (red curve) are characterized by separated strong signals in the range between 1650 cm^{-1} and 1250 cm^{-1} . This is characteristic for a sp^2 -hybridized heterocycle with the signals at 1605 cm^{-1} and 1564 cm^{-1} corresponding to C=N bonds and the

signals at 1416 cm^{-1} , 1305 cm^{-1} and 1241 cm^{-1} assignable to C-N bonds. Furthermore, the characteristic fingerprint signal of the triazine unit at 809 cm^{-1} is clearly visible, indicating the formation of stoichiometric C_3N_4 .^[46c, 48] To confirm the conclusions drawn from IR and gain information of the amount of nitrogen incorporation, we investigated the exact binding situation within the materials by X-ray photoelectron spectroscopy (XPS) given in **Figure 5**. Quantitative analysis reveals an atomic C/N ratio of 1.61 for C@N expected for nitrogen doped carbons synthesized at low carbonization temperatures.^[59] Accordingly, we expect the occurrence of distinguishable energy levels for nitrogen atoms as schematically shown in **Figure 5a**. The N 1s region (**Figure 5b**) shows contributions at 398.1 eV, which can be assigned to pyridinic nitrogen species (shown in magenta), and 399.6 eV characteristic for pyrrolic nitrogen species shown in green respectively.^[60] In the C 1s region (**Figure 5c**) two species can be observed as well. The signal at 284.8 eV is characteristic of C=C bonds while the second contribution at 287.2 eV can be assigned to carbon atoms bound to nitrogen.

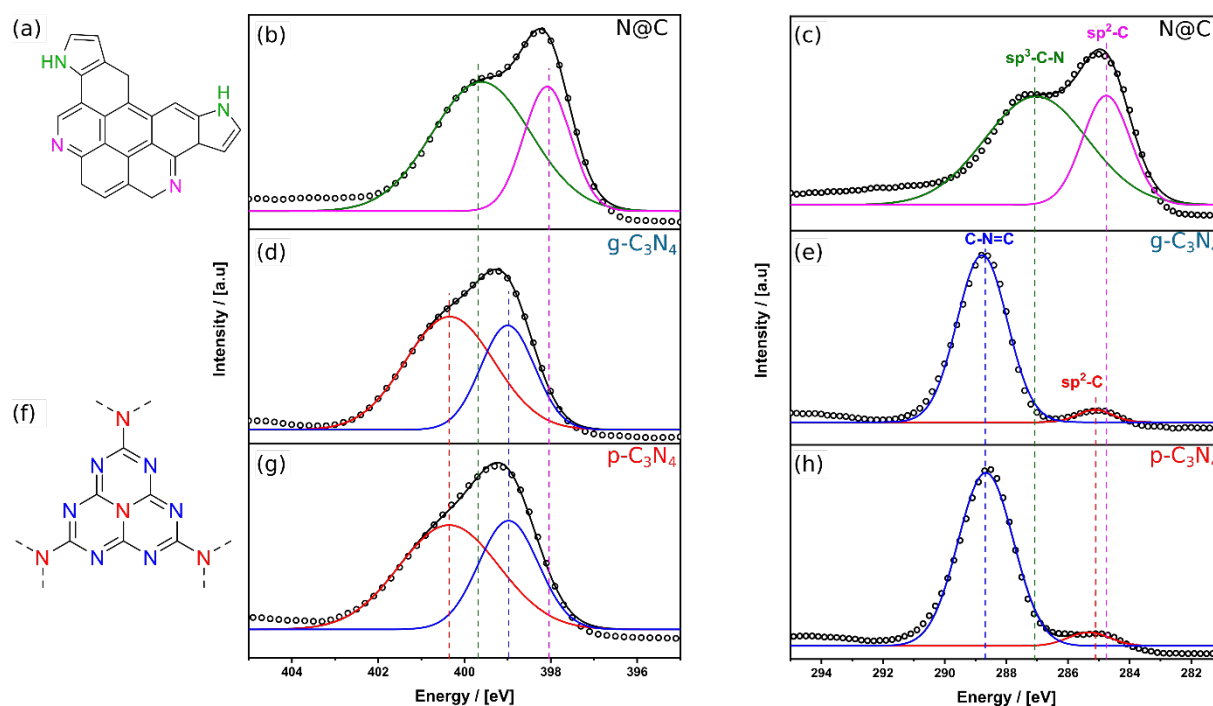


Figure 5: (a) Schematic depiction of the chemical structure of nitrogen doped carbon. Detailed XPS spectra for N@C of the (b) N 1s region and (c) C 1s region. Detailed XPS spectra for g-C₃N₄ of the (d) N 1s region and (e) C 1s region. (f) Schematic depiction of the chemical structure of carbon nitride. Detailed XPS spectra for g-C₃N₄ of the (g) N 1s region and (h) C 1s region.

This binding situation in N@C is clearly distinguishable from the stoichiometric carbon nitride compound g-C₃N₄ and p-C₃N₄. The corresponding N 1s spectra (**Figure 5(d),(g)**) are composed of two equivalently contributing species. The signal detected at 400.3 eV (red curve) can be assigned to nitrogen atoms bound to three carbon atoms while the contribution at 399.0 eV (blue curve) is characteristic for sp²-hybridized nitrogen atoms in the heterocyclic ring forming C-N=C-bonds. In comparison, the fraction of N-C₃ species is slightly reduced for p-C₃N₄. The C 1s region (**Figure 5e**) shows characteristic energy levels for carbon atoms bound to three nitrogen atoms in heterocycles at 288.8 eV. Only a minor component at 285.1 eV caused by C-C bonds, likely located at surface defects, can be detected. As the atomic ratio C/N is calculated to be 0.73 for g-C₃N₄, we propose a structure close to the ideal heptazine-based polymer shown in **Figure 5f**.^[61] For p-C₃N₄, the signal corresponding to carbon atoms in the triazine unit (blue curve in **Figure 5h**) is slightly shifted to 288.6 eV indicating a change in binding situation. As the atomic C/N ratio is enhanced to 0.75, we attribute this to the formation of a triazine-heptazine polymer as reported previously in literature.^[44c, 62] The crystalline structure determined by powder X-ray diffraction (PXRD) measurements (Supporting Information **Figure S14**) showing a very broad reflex, corresponding to the interplane stacking expected for the synthesized materials. The observed shift of the (002)-reflex to higher interlayer distances for C@N as compared to g-C₃N₄ and p-C₃N₄, consistent with the proposed structures and confirms the determined structures.

2.4. Optical Properties and modification of graded porous materials.

As a final distinction between the synthesized materials, we investigated their optical properties using solid-state UV-VIS spectroscopy (**Figure 6(a)**). As the application fields for doped carbons asks for high conductivity^[39, 41b, 63], while g-C₃N₄ is mainly discussed in photocatalysis^[46b, 64], the modification of the electronic structure is highly important for future

applications. We herein show the first synthetic route capable of creating graded nanoporous materials exhibiting these highly adjustable properties. This is demonstrated by a comparison of the synthesized N@C, g-C₃N₄ and p-C₃N₄ with different internal structures. In accordance with the determined structure of a sp²-hybridized nitrogen doped carbon material, N@C (Supporting Information **Figure S15**) is characterized by a strong absorbance over the whole visible range. In contrast, g-C₃N₄ materials (blue curves) show an absorption in the visible range starting from ~500 nm. Importantly, the band gap of g-C₃N₄ can be modified by the usage of different precursor systems, as this results in slightly altered C/N ratios and therefore a modified binding situation.^[65] This concept can be transferred to tailored gradient porous C₃N₄ materials, as shown by the synthesis of g-C₃N₄ using pure cyanamide or cyanamide-guanidine mixtures (see Supporting Information **Fig. S16**) as precursors. The resulting gradient porous monoliths are characterized by shifted band gaps in the range 2.55 eV and 2.77 eV as calculated from Tauc plots (inset in **Figure 6(a)**).

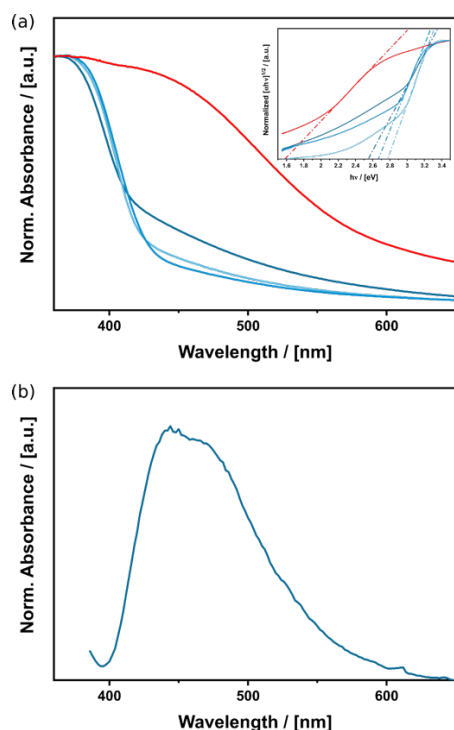


Figure 1: Solid state UV-VIS absorption measurements (a) normalized to the absorbance at 366 nm with Tauc plots as inset of the g-C₃N₄ samples (blue) synthesized using mixtures of cyanamide-urea mixture (dark blue), cyanamide-guanidine mixtures (blue) and pure cyanamide (light blue) and p-C₃N₄ (red) and a representative PL spectrum of g-C₃N₄.

As matching photonic properties with the electronic band gap can lead to highly enhanced photoelectronic features^[7], the independent adjustment of pore sizes and electronic properties is highly important. Therefore, the modified optical properties of g-C₃N₄ (red curve), shown by the broadened and red shifted absorbance in the solid state, are important. This results in a shift of the optical band gap to a comparable low value of 1.63 eV (inset in **Figure 6**). This is a result of the desired triazine-heptazine based polymeric structure, realized by a deliberately chosen precursor approach, resulting in the formation of a donor-acceptor structure^[44a, 62], showing the tailored variability of the optical properties in semiconducting materials with gradient porosity. For proof of concept, we have recorded photoluminescence (PL) spectra of a representative case (**Figure 6(b)**). As expected, the emission signal ($\lambda_{\text{max}} = 443\text{nm}$) is red shifted with respect to the adsorption edge.

3. Conclusion

Possible applications of gradient porous materials have been limited due to a lack of synthetic methods. We use preparative ultracentrifugation as a powerful tool to overcome this issue. By carefully analyzing the sedimentation parameters and a subsequent transfer towards PUC, SiO₂-NPs can be fractionated in water or concentrated precursor-solutions. The formed colloidal glasses with gradually changing particles size along the direction of the centrifugal force can then be directly used as templating structures, which was not possible until now. We demonstrate this by developing a highly flexible synthetic method towards graded porous materials ranging from carbon over nitrogen doped carbon to C₃N₄, which was not possible so far. In addition to the described synthesis methods, relying on aqueous systems, SiO₂-NPs offer the advantage of a compatibility with various dispersion media, making a wide range of precursors applicable, as shown by the synthesis of g-C₃N₄ and p-C₃N₄ with significantly altered properties. A further combination with our previous finding of the possibility of the

introduction of chemical gradients into carbon materials by PUC^[50-51], will allow the synthesis of tailor made catalysts exhibiting graded porosity, significantly enhancing the field and possible applications of FGM.

Since local concentration and the control of mass and photon propagation is an important factor for catalytic processes^[66], we propose that the herein described materials offer an ideal platform to investigate possible synergistic effects in heterogeneous electro- and photocatalysis. Especially the investigations on the impact of a gradient in pore sizes on the optical properties and light propagation in our synthesized materials will allow an improvement of photocatalytic activity, for example by highly localized light trapping.^[67] Due to the high refractive index of C₃N₄, a resonant light transport seems likely for pore sizes in the range of visible light^[18b]. In combination with prolonged retention times of photons inside of photonic glasses^[18a] an enhancement in light harvesting is to be expected, if the photonic structure, resulting as a function of the pore sizes matches the energy levels of the electronic band gap. However, as our study is, to the best of our knowledge, the first report of a gradient porous semiconductors with pore sizes in the regime of the visible light, the necessary complex measurement setups will have to be developed first, which asks for further research.

4. Experimental Section/Methods

Materials. Tetraethylorthosilicate (TEOS, > 98 %), cyanamide (>99 %), 5-aminotetrazole (5AT, >97 %) and dicyandiamide (>99 %) were purchased from Sigma-Aldrich. Guanidine carbonate (>98 %) and melamine (>99 %) were purchased at abcr. Resorcinol (>99 %) and urea (>99.5 %) were purchased from Merck. Aqueous formaldehyde solution (37 wt%) was purchased from Roth. Guanidine hydrochloride (>98 %) was purchased from Alfa Aesar.

Preparation of template particles. SiO₂-Nanoparticles were synthesized by the Stoeber method.^[53] SiO₂-129 was synthesized by first dissolving concentrated aqueous NH₄OH-

solution (4.5 mL) in ethanol (100 mL). The solution was heated to 60°C under stirring. After 30 min, TEOS (4.5 mL) was rapidly injected into the solution. The reaction was allowed to proceed for 24 h. SiO₂-129 was isolated by centrifugation and washed 2 times with Ethanol and subsequently 2 times with water. The obtained powder was dried and then dispersed and stored in water. The solid content was determined to be 11.8 wt%. SiO₂-310 was synthesized by heating a solution of MilliQ-grade water (72 mL), concentrated aqueous NH₄OH-solution (15 mL) and ethanol (100 mL) 60 °C. The solution was heated to 30°C under stirring. After 30 min, TEOS (20 mL) was rapidly injected into the solution. The reaction was allowed to proceed for 2 h. SiO₂-310 was isolated by centrifugation and washed 2 times with Ethanol and subsequently 2 times with water. The obtained powder was dried and then dispersed and stored in water. The solid content was determined to be 10.6 wt%.

Preparation of SiO₂-Assemblies. Dispersions of SiO₂-129 and SiO₂-310 were mixed in a volumetric ratio of 1:1 and diluted with MilliQ-grade water. The samples were then fractionated in thickwall polypropylene (13×51 mm) centrifuge tubes by ultracentrifugation using a Beckman a Beckman Optima L-70 ultracentrifuge (Beckman instruments) equipped with a swinging-bucket rotor (SW 55 Ti, Beckman Instruments). For the detailed parameters (Volume ratios, centrifugal force), see the Supporting Info. After centrifugation, the supernatant was carefully removed, and the samples were dried at ambient conditions.

Preparation of gradient porous materials by melt infiltration. SiO₂ assemblies formed after PUC were overlayed with excess 5AT in a corundum crucible. The sample was heated to 550 °C over 12 h. During heat up, the monoliths were infiltrated. The full conversion to g-C₃N₄ was achieved after holding the temperature at 550 °C for 2 h. After cooling down, SiO₂ was removed from the monolithic composites by etching in aqueous 20 wt% HF-solutions. After washing of the material with water, monolithic porous materials were obtained after drying at 90 °C under ambient pressure.

Preparation of gradient porous materials by in-situ infiltration. For materials synthesis, aqueous dispersions of SiO₂-129 and SiO₂-310 (volumetric ratio of 1:1) were mixed with the respective concentrated precursor solutions (see the Supporting Info detailed parameters). The samples were infiltrated during fractionation in thickwall polypropylene (13 mm×51 mm) centrifuge tubes by ultracentrifugation using a Beckman a Beckman Optima L-70 ultracentrifuge (Beckman instruments) equipped with a swinging-bucket rotor (SW 55 Ti, Beckman Instruments). After centrifugation, the supernatant was carefully removed and the samples were dried at 90 °C for 3 days. The resulting monolithic, infiltrated samples were then pyrolyzed in a nitrogen atmosphere at 550 °C for 2 h with a heating ramp over 12 h. After cooling down, SiO₂ was removed from the monolithic composites by etching in aqueous 20 wt% HF-solutions. After washing of the material with water, monolithic porous materials were obtained after drying at 90 °C under ambient pressure.

Materials Characterization. For SEM imaging, monolithic carbon samples were cut into two pieces along the direction of the centrifugal force. Images were then acquired at several positions along the resulting cross-section using a Zeiss Gemini SEM 500 operating at 3-15 kV. EDX data were recorded using an Oxford Instruments Ultim[®] Max with a 100 mm² Silicon Drift Detector mounted onto the microscope. X-ray diffraction analysis was performed with a Bruker AXS D8 Advance diffractometer using Cu-K α radiation. TGA-measurements were performed using a Netzsch STA 429 F3 Jupiter. XPS measurements were performed by Tascon GmbH, Sulzbach, Germany using a PHI Quantera SXM with Al- K α radiation. FT-IR spectra were obtained with a Perkin-Elmer Spectrum 100 with ATR measurement unit. N₂-physisorption measurements were conducted on a Micromeritics TriStar 3000. UV VIS measurements were recorded using a Cary-5000 including integrated sphere, Agilent 8453. AUC measurements were conducted using an Optima XL-I analytical ultracentrifuge (Beckman Coulter, Palo Alto, CA, USA) with Rayleigh interference optics in a titanium measurement cell (Nanolytics, Potsdam, Germany). The optical pathway length of the cell was 12 mm.

Supporting Information

Supporting Information is available from the Web or from the author.

Acknowledgements

We thank the Carl-Zeiss foundation for funding Jochen Bahner by a full Ph. D.scholarship. We gratefully acknowledge technical/instrumental support from the German Research Foundation (DFG) via SFB1214 Project Z1 Particle Analysis Center. We acknowledge Rose Rosenberg for assisting in AUC measurements. The authors thank Nele Klinkenberg, Ulrich Bahnmüller and Sebastian Sutter for their valuable feedback from proofreading the manuscript.

References

- [1] a) M. Hartmann and W. Schwieger, *Chem Soc Rev* **2016**, *45*, 3311-3312; b) Y. Li, Z.-Y. Fu and B.-L. Su, *Advanced Functional Materials* **2012**, *22*, 4634-4667.
- [2] M. H. Sun, S. Z. Huang, L. H. Chen, Y. Li, X. Y. Yang, Z. Y. Yuan and B. L. Su, *Chem Soc Rev* **2016**, *45*, 3479-3563.
- [3] C. M. Parlett, K. Wilson and A. F. Lee, *Chem Soc Rev* **2013**, *42*, 3876-3893.
- [4] a) S. Polarz and M. Antonietti, *Chemical Communications* **2002**, 2593-2604; b) O. D. Velev and E. W. Kaler, *Advanced Materials* **2000**, *12*, 531-534.
- [5] E. Yablonovitch, T. J. Gmitter and K. M. Leung, *Physical Review Letters* **1991**, *67*, 2295-2298.
- [6] J. C. Knight, *Nature* **2003**, *424*, 847-851.
- [7] E. Armstrong and C. O'Dwyer, *Journal of Materials Chemistry C* **2015**, *3*, 6109-6143.
- [8] F. Temerov, B. Ankudze and J. J. Saarinen, *Materials Chemistry and Physics* **2020**, *242*, 122471.
- [9] L. Zheng, H. Cheng, F. Liang, S. Shu, C. K. Tsang, H. Li, S.-T. Lee and Y. Y. Li, *Journal of Physical Chemistry C* **2012**, *116*, 5509-5515.
- [10] J. I. L. Chen and G. A. Ozin, *Journal of Materials Chemistry* **2009**, *19*, 2675-2678.
- [11] X. Zhang and S. John, *Journal of Materials Chemistry A* **2020**, *8*, 18974-18986.

- [12] a) J. Liu, H. Zhao, M. Wu, B. Van der Schueren, Y. Li, O. Deparis, J. Ye, G. A. Ozin, T. Hasan and B.-L. Su, *Advanced Materials* **2017**, *29*, 1605349; b) S. Y. Lim, C. S. Law, M. Markovic, J. K. Kirby, A. D. Abell and A. Santos, *ACS Applied Materials & Interfaces* **2018**, *10*, 24124-24136.
- [13] J. Low, L. Zhang, B. Zhu, Z. Liu and J. Yu, *ACS Sustainable Chemistry & Engineering* **2018**, *6*, 15653-15661.
- [14] P. D. Garcia, R. Sapienza and C. Lopez, *Adv Mater* **2010**, *22*, 12-19.
- [15] M. Gaio, M. Peruzzo and R. Sapienza, *Optics Letters* **2015**, *40*, 1611-1614.
- [16] L. Schertel, L. Siedentop, J.-M. Meijer, P. Keim, C. M. Aegerter, G. J. Aubry and G. Maret, *Advanced Optical Materials* **2019**, *7*, 1900442.
- [17] P. W. Anderson, *Philosophical Magazine B* **1985**, *52*, 505-509.
- [18] a) M. Chen, D. Fischli, L. Schertel, G. J. Aubry, B. Häusele, S. Polarz, G. Maret and H. Cölfen, *Small* **2017**, *13*, 1701392; b) L. Schertel, I. Wimmer, P. Besirske, C. M. Aegerter, G. Maret, S. Polarz and G. J. Aubry, *Physical Review Materials* **2019**, *3*, 015203.
- [19] a) J. J. do Rosário, P. N. Dyachenko, R. Kubrin, R. M. Pasquarelli, A. Y. Petrov, M. Eich and G. A. Schneider, *ACS Applied Materials & Interfaces* **2014**, *6*, 12335-12345; b) S.-H. Kim, S. Magkiriadou, D. K. Rhee, D. S. Lee, P. J. Yoo, V. N. Manoharan and G.-R. Yi, *ACS Applied Materials & Interfaces* **2017**, *9*, 24155-24160.
- [20] G. H. Lee, J. Y. Sim and S.-H. Kim, *ACS Applied Materials & Interfaces* **2016**, *8*, 12473-12480.
- [21] Y. Häntsch, G. Shang, A. Petrov, M. Eich and G. A. Schneider, *Advanced Optical Materials* **2019**, *7*, 1900428.
- [22] B. H. Rabin and I. Shiota, *MRS Bulletin* **1995**, *20*, 14-18.
- [23] J. Genzer, *Annual Review of Materials Research* **2012**, *42*, 435-468.
- [24] a) W. Du and C. Gao, *Macromol Biosci* **2019**, *19*, e1900292; b) Z. Wang, *ACS Nano* **2018**, *12*, 1273-1284.

- [25] M. M. Collinson and D. A. Higgins, *Langmuir* **2017**, *33*, 13719-13732.
- [26] J. Werner, B. Linner-Krčmar, W. Friess and P. Greil, *Biomaterials* **2002**, *23*, 4285-4294.
- [27] P. Fratzl and R. Weinkamer, *Progress in Materials Science* **2007**, *52*, 1263-1334.
- [28] X. Miao and D. Sun, *Materials* **2009**, *3*, 26-47.
- [29] T. Yamaoka, *Analytica Chimica Acta* **1998**, *372*, 91-98.
- [30] a) J. E. Trachtenberg, J. K. Placone, B. T. Smith, J. P. Fisher and A. G. Mikos, *J Biomater Sci Polym Ed* **2017**, *28*, 532-554; b) S. Sultan and A. P. Mathew, *Nanoscale* **2018**, *10*, 4421-4431.
- [31] a) A. Ahmed, J. Smith and H. Zhang, *Chemical Communications* **2011**, *47*, 11754-11756; b) C. Stubenrauch, A. Menner, A. Bismarck and W. Drenckhan, *Angewandte Chemie International Edition* **2018**, *57*, 10024-10032.
- [32] a) P. Gannon, S. Sofie, M. Deibert, R. Smith and V. Gorokhovskiy, *Journal of Applied Electrochemistry* **2008**, *39*, 497-502; b) A. Macchetta, I. G. Turner and C. R. Bowen, *Acta Biomaterialia* **2009**, *5*, 1319-1327.
- [33] M. Costantini, J. Jaroszewicz, Ł. Kozoń, K. Szlązak, W. Świąszkowski, P. Garstecki, C. Stubenrauch, A. Barbetta and J. Guzowski, *Angewandte Chemie International Edition* **2019**, *58*, 7620-7625.
- [34] D. Tan, Q. Li, B. Yang, X. Wang, S. Hu, Z. Wang, Y. Lei and L. Xue, *Langmuir* **2019**, *35*, 5864-5870.
- [35] a) A. Spinnrock and H. Colfen, *Chemistry- A European Journal* **2019**, *25*, 10026-10032; b) X. Xu and H. Colfen, *Nanomaterials* **2021**, *11*.
- [36] a) X. Xu and H. Colfen, *ChemPhysChem* **2019**, *20*, 1799-1803; b) X. Xu, T. Franke, K. Schilling, N. Sommerdijk and H. Colfen, *Nano Lett* **2019**, *19*, 1136-1142.
- [37] M. Chen, H. Cölfen and S. Polarz, *ACS Nano* **2015**, *9*, 6944-6950.
- [38] M. Chen, K. Hagedorn, H. Colfen and S. Polarz, *Adv Mater* **2017**, *29*.
- [39] J. P. Paraknowitsch and A. Thomas, *Energy & Environmental Science* **2013**, *6*.

- [40] W. Shen and W. Fan, *J. Mater. Chem. A* **2013**, *1*, 999-1013.
- [41] a) E. Luo, M. Xiao, J. Ge, C. Liu and W. Xing, *J. Mater. Chem. A* **2017**, *5*, 21709-21714; b) D. Guo, H. Wei, X. Chen, M. Liu, F. Ding, Z. Yang, Y. Yang, S. Wang, K. Yang and S. Huang, *Journal of Materials Chemistry A* **2017**, *5*, 18193-18206; c) Z. Yi, Z. Zhang, S. Wang and G. Shi, *Journal of Materials Chemistry A* **2017**, *5*, 519-523.
- [42] H. Wang, J. Jia, P. Song, Q. Wang, D. Li, S. Min, C. Qian, L. Wang, Y. F. Li, C. Ma, T. Wu, J. Yuan, M. Antonietti and G. A. Ozin, *Angew Chem Int Ed Engl* **2017**, *56*, 7847-7852.
- [43] K. Ogata, J. F. D. Chubaci and F. Fujimoto, *Journal of Applied Physics* **1994**, *76*, 3791-3796.
- [44] a) D. Dontsova, S. Pronkin, M. Wehle, Z. Chen, C. Fettkenhauer, G. Clavel and M. Antonietti, *Chemistry of Materials* **2015**, *27*, 5170-5179; b) A. Savateev, S. Pronkin, J. D. Epping, M. G. Willinger, C. Wolff, D. Neher, M. Antonietti and D. Dontsova, *ChemCatChem* **2017**, *9*, 167-174; c) G. Zhang, M. Liu, T. Heil, S. Zafeiratos, A. Savateev, M. Antonietti and X. Wang, *Angewandte Chemie International Edition* **2019**, *58*, 14950-14954.
- [45] Y. Wang, X. Wang and M. Antonietti, *Angewandte Chemie International Edition* **2012**, *51*, 68-89.
- [46] a) A. Kumar, P. Raizada, P. Singh, R. V. Saini, A. K. Saini and A. Hosseini-Bandegharai, *Chemical Engineering Journal* **2020**, *391*, 123496; b) K. R. Reddy, C. H. V. Reddy, M. N. Nadagouda, N. P. Shetti, S. Jaesool and T. M. Aminabhavi, *Journal of Environmental Management* **2019**, *238*, 25-40; c) J. Oh, J. M. Lee, Y. Yoo, J. Kim, S.-J. Hwang and S. Park, *Applied Catalysis B: Environmental* **2017**, *218*, 349-358; d) A. Mishra, A. Mehta, S. Basu, N. P. Shetti, K. R. Reddy and T. M. Aminabhavi, *Carbon* **2019**, *149*, 693-721; e) P. Lianos, *Applied Catalysis B: Environmental* **2017**, *210*, 235-254; f) W. Zhan, L. Sun and X. Han, *Nano-Micro Letters* **2019**, *11*; g) Y. Shi, J. Huang, G. Zeng, W. Cheng and J. Hu, *Journal of Membrane Science* **2019**, *584*, 364-392; h) J. H. Pan, H. Dou, Z. Xiong, C. Xu, J. Ma and X. S. Zhao, *Journal of Materials Chemistry* **2010**, *20*.

- [47] a) Y. Li, X. Li, H. Zhang and Q. Xiang, *Nanoscale Horiz* **2020**, *5*, 765-786; b) S. N. Talapaneni, G. Singh, I. Y. Kim, K. AlBahily, A. H. Al-Muhtaseb, A. S. Karakoti, E. Tavakkoli and A. Vinu, *Adv Mater* **2020**, *32*, e1904635.
- [48] Q. Liang, Z. Li, X. Yu, Z.-H. Huang, F. Kang and Q.-H. Yang, *Advanced Materials* **2015**, *27*, 4634-4639.
- [49] L. Sun, M. Yang, J. Huang, D. Yu, W. Hong and X. Chen, *Advanced Functional Materials* **2016**, *26*, 4943-4950.
- [50] J. Bahner, N. Klinkenberg, M. Frisch, L. Brauchle and S. Polarz, *Advanced Functional Materials* **2019**, *29*, 1904058.
- [51] J. Bahner, N. Hug and S. Polarz, *C* **2021**, *7*, 22.
- [52] a) X. Fan, Z. Xing, Z. Shu, L. Zhang, L. Wang and J. Shi, *RSC Advances* **2015**, *5*, 8323-8328; b) K. Muirhead, S. Earnshaw, C. J. Easton and A. Philbrook, *Journal of Applied Polymer Science* **2012**, *125*, E372-E377.
- [53] W. Stöber, A. Fink and E. Bohn, *Journal of Colloid and Interface Science* **1968**, *26*, 62-69.
- [54] O. D. Velev and S. Gupta, *Advanced Materials* **2009**, *21*, 1897-1905.
- [55] R. Piazza, S. Buzzaccaro, E. Secchi and A. Parola, *Phys Biol* **2013**, *10*, 045005.
- [56] I. Arganda-Carreras, V. Kaynig, C. Rueden, K. W. Eliceiri, J. Schindelin, A. Cardona and H. Sebastian Seung, *Bioinformatics* **2017**, *33*, 2424-2426.
- [57] C. T. Rueden, J. Schindelin, M. C. Hiner, B. E. DeZonia, A. E. Walter, E. T. Arena and K. W. Eliceiri, *BMC Bioinformatics* **2017**, *18*, 529.
- [58] K. Sakaushi and M. Antonietti, *Bulletin of the Chemical Society of Japan* **2015**, *88*, 386-398.
- [59] S. Zhang, S. Tsuzuki, K. Ueno, K. Dokko and M. Watanabe, *Angew Chem Int Ed Engl* **2015**, *54*, 1302-1306.

- [60] M. Ayiania, M. Smith, A. J. R. Hensley, L. Scudiero, J.-S. McEwen and M. Garcia-Perez, *Carbon* **2020**, *162*, 528-544.
- [61] N. Hellgren, R. T. Haasch, S. Schmidt, L. Hultman and I. Petrov, *Carbon* **2016**, *108*, 242-252.
- [62] G. Zhang, L. Lin, G. Li, Y. Zhang, A. Savateev, S. Zafeiratos, X. Wang and M. Antonietti, *Angew Chem Int Ed Engl* **2018**, *57*, 9372-9376.
- [63] S. Dutta, A. Bhaumik and K. C. W. Wu, *Energy Environ. Sci.* **2014**, *7*, 3574-3592.
- [64] L. Jiang, X. Yuan, Y. Pan, J. Liang, G. Zeng, Z. Wu and H. Wang, *Applied Catalysis B: Environmental* **2017**, *217*, 388-406.
- [65] Z. Yang, K. Hu, X. Meng, Q. Tao, J. Dong, B. Liu, Q. Lu, H. Zhang, B. Sundqvist, P. Zhu, M. Yao and B. b. Liu, *Carbon* **2018**, *130*, 170-177.
- [66] W. Wan, R. Zhang, M. Ma and Y. Zhou, *Journal of Materials Chemistry A* **2018**, *6*, 754-775.
- [67] X. Sheng, J. Liu, I. Kozinsky, A. M. Agarwal, J. Michel and L. C. Kimerling, *Advanced Materials* **2011**, *23*, 843-847.